Composites: Part A 196 (2025) 109010

Contents lists available at ScienceDirect

Composites Part A

journal homepage: www.elsevier.com/locate/compositesa

Poly(butylene adipate-co-terephthalate) as a new healing agent for epoxy/basalt composites

Laura Simonini [a,b,*], Daniele Rigotti [a,b], Jeevan Kishore Reddy Pidapa [a], Alessandro Pegoretti [a,b]

[a] Department of Industrial Engineering, University of Trento, Via Sommarive 9, 38121 Trento, Italy
[b] National Interuniversity Consortium of Materials Science and Technology (INSTM), Via Giusti 9, 50121 Florence, Italy

HIGHLIGHTS

- PBAT and PCL coatings were obtained by fluid coating from polymer solutions.
- SEM analysis revealed smooth coatings at low speeds and droplet formation at higher speeds.
- IFSS remained consistent across the coated and uncoated samples, maintaining strong fiber–matrix adhesion.
- Nearly complete interfacial self-healing was achieved with PBAT and PCL coatings.

ARTICLE INFO

Keywords:
Basalt
Thermoplastic
Interface
Self-healing
Composite

ABSTRACT

The aim of this work was to demonstrate that interfacial healing in epoxy/basalt composites can be achieved by coating basalt fibres with thermoplastic polymer poly(butylene adipate-co-terephthalate) (PBAT). As a reference healing agent, the widely studied polycaprolactone (PCL) was also used to coat the basalt fibres. The two polymers were applied by fluid coating from polymer solutions at different coating speeds. Scanning electron microscopy revealed smooth and high quality coatings for both polymers at low coating speeds. At higher coating speeds (>20 mm/s), PCL behaved like a Newtonian fluid, forming droplet-like structures. PBAT, on the other hand, behaved like a non-Newtonian shear-thinning fluid, forming droplets at speeds above 80 mm/s. Contact angle measurements showed a significant reduction in contact angle hysteresis (θ_H) for fibers coated with both polymers compared to uncoated, with PBAT exhibiting the lowest θ_H and a smoother surface. The coated fibers were then combined with an epoxy matrix to form microcomposites and tested in a microdebonding configuration to measure the interfacial shear strength (IFSS). Moreover, the fiber/matrix interface was healed by a 30 min thermal treatment at 80 °C for PCL and at 120 °C for PBAT and healing efficiency (HE) parameter was evaluated by repeating the microdebonding test. With the new PBAT coating HE values up to 89.5 % were obtained, very similar to the HE values of up to 93.8 % achieved with the reference PCL coating. In conclusion, PBAT coating resulted to be a promising alternative candidate to PCL to reach interfacial healing in basalt fibers reinforced epoxy composites.

1. Introduction

Fiber-reinforced composites (FRCs) have transformed the modern engineering and manufacturing due to their exceptional strength-to-weight ratio, tailored mechanical properties and versatility in a variety of applications, including aerospace [1], automotive [2], construction [3] and renewable resources sectors [4]. Their performance and reliability depend on the integrity of the fiber/matrix interface, which acts as a critical region for load transfer, stress distribution and energy dissipation during mechanical loading [5–7]. Weak or degraded interfaces can lead to interfacial debonding, micro-fractures and ultimately composite failure under mechanical or environmental stress [8–11]. Consequently, the improvement of interfacial properties has become a key element of composite materials research.

Among the various strategies to improve the fiber/matrix interface [8,12–15], the development of functional coatings for fibers has

* Corresponding author at: Department of Industrial Engineering, University of Trento, Via Sommarive 9, 38121 Trento, Italy.
E-mail address: laura.simonini@unitn.it (L. Simonini).

https://doi.org/10.1016/j.compositesa.2025.109010
Received 10 March 2025; Received in revised form 23 April 2025; Accepted 5 May 2025
Available online 6 May 2025

emerged as a highly effective and versatile solution [16–18]. Fiber coatings can be designed to improve interfacial adhesion by the modification of the surface energy, the introduction of functional groups for chemical bonding or the creation of tailored surface morphologies to increase mechanical interlocking [19,20]. In particular, thermoplastic polymer coatings have attracted significant attention for their ability not only to improve interfacial adhesion, but also to impart self-healing capabilities to the composite interface [21]. Self-healing interfaces represent a biomimetic approach to damage management, enabling the repair of micro-fractures and interfacial defects under controlled stimuli such as heat or pressure [22,23]. This capability greatly extends the lifespan of composite materials, reduces maintenance costs and increases sustainability by mitigating premature material failure [24].

Basalt fibers (BFs) have emerged as a promising reinforcement material for composite applications due to their superior mechanical properties, excellent thermal and chemical resistance and environmentally friendly production process [25]. Derived from natural volcanic rocks, basalt fibers offer a sustainable alternative to traditional reinforcements such as glass and carbon fibers, making them particularly attractive for applications requiring high strength and environmental compatibility [26]. However, as with other fibers, interfacial bonding with polymer matrices can present challenges, especially due to the smooth and inert nature of their surfaces [14,27]. The application of thermoplastic polymer coatings could provide an effective strategy to improve the interfacial performance by promoting better adhesion, reducing stress concentrations and introducing functional properties such as self-healing capability [28–34]. In this scenario, polycaprolactone (PCL) has been widely used as an healing agent for bulk epoxy system [35–37] and more recently also as a healable coating for glass [21,28] and carbon fibers [38] embedded in an epoxy matrix. Among semicrystalline thermoplastic polymers poly(butylene adipate-co-terephthalate) (PBAT) has great potential as an healing agent for fiber coatings in composite systems due to its relative low melting temperature (about 115 °C) and low viscosity in the molten state [39,40]. PBAT is a copolymer with high toughness, ductility and biodegradability characteristics, commonly used in sustainable applications [41]. Both PBAT and PCL can be transformed into thin, uniform coatings, to provide interfacial properties and maintaining compatibility with various polymer matrices [42,43].

The coating of fibers with such thermoplastic polymers can be achieved according to the fluid coating, which provides a comprehensive model to control the deposition of polymer layers onto the fiber surfaces [44]. Fluid coating occurs when a viscous fluid is forced to deposit on a moving solid object, which in this case are represented by the polymer dissolved in liquid solution and the fibers, respectively [45,46]. Fluid coating considers factors such as fiber surface tension, coating viscosity and fiber moving speed to achieve uniform, defect-free coatings. The achievement of optimal coatings is critical, as the thickness, uniformity and adhesion of the coating directly influence the interfacial properties and overall performance of the composite.

Therefore, for the first time, the aim of this work was to enhance the interfacial properties of FRCs through the use of PBAT thermoplastic coatings on BFs and to compare the performances with those achievable with a reference material for the healing of epoxy resins such as PCL. These polymers were applied onto the fibers by fluid coating and the resulting coatings were analysed for their physical and microstructural characteristics. Furthermore, the interfacial adhesion between the fibers and the matrix and the interfacial self-healing efficiency were evaluated using microdebonding tests.

2. Experimental part

2.1. Materials

BAS 220P basalt fibers were supplied by Basaltex Nv. (Wevelgem, Belgium) as a plain fabric from which individual fibers were manually extracted. The fabric had an air weight of 220 g/m^2 and an average fiber diameter of 15 μm. The fibers had melting temperature of 1350 °C and uncoated filament density of 2.67 g/cm^3. They were received with an epoxy compatible silane based sizing.

PCL was supplied by Polysciences Inc. (Warrington, PA, USA) as pellets (average diameter 3 mm) with a density of 1.12 g/cm^3 and a molecular weight (M_w) of 80,000 g/mol. It exhibited a glass transition temperature of −68 °C and a melting temperature of 59 °C.

PBAT Technipol® Bio 1160 was supplied by Sipol Spa (Mortara, PV, Italy) as pellets (average diameter 3 mm) with density of 1.23 g/cm^3 and M_w of 52,000 g/mol. It exhibited a glass transition temperature of −37 °C and a melting temperature of 115 °C.

Epoxy resin (EC 157.1) and an amine-based hardener (W 342) were supplied by Elantas Italia S.r.l. (Collecchio, Italy). The two components were mixed at a weight ratio of 100:30 and cured for 40 h at 50 °C, based on the optimized procedure assessed in preliminary works [39]. The cured epoxy had a glass transition temperature of 84 °C, a thermal degradation temperature of 352 °C, an elastic modulus of 3.1 ± 0.2 GPa, and a tensile strength of 60.7 ± 15.3 MPa.

Dimethylformamide (DMF), having density of 0.94 g/cm^3 and purity of 99.8 %, and tetrahydrofuran (THF) having density of 0.89 g/cm^3 and purity of 99.9 % were purchased by Sigma Aldrich Co. (Missouri, USA) and were used as solvents for PCL and PBAT. All materials were utilized as received.

2.2. Sample preparation

2.2.1. Preparation of polymer solutions

PCL and PBAT were dissolved separately in a 30:70 wt% mixture of DMF:THF in order to obtain two liquid solutions each containing 10 wt% of PCL or PBAT. The solutions were stirred at room temperature for 4 h at 300 rpm until the polymers were completely dissolved.

2.2.2. Preparation of coated fibers

The deposition of the coatings on the fibers was performed using a custom-built apparatus (Fig. 1a), and the coating process followed the fluid coating theory, previously explained by Simonini et al. [21].

A single basalt fiber was attached to a sample holder made of poly (methyl methacrylate) (PMMA) using UV light-cured adhesive and guided through a droplet of polymer solution, which was manually deposited on a fixed perforated PMMA frame using a syringe (Fig. 1b).

The sample holder was mounted on a linear guide system that allowed translation along the fiber axis at a constant speed. Movement was driven by a helical lead screw actuated by a stepper motor controlled via an Arduino microcontroller. The speed of coating was controlled via Arduino and set in the range from 1.5 to 100 mm/s. The speed and displacement of the system were calibrated using a dial indicator and validated through video recordings. Precise alignment of the polymer application hole was achieved using two microscopes, a Thorlabs microscope (Thorlabs Inc., Newton, New Jersey, United States) and a Dino-Lite microscope (AnMo Electronics Corporation, New Taipei City, Taiwan). The samples codes are summarized in Table 1.

2.3. Experimental techniques

2.3.1. Rheological measurements

The rheological properties of the PCL and PBAT solutions were investigated using a Discovery hybrid rheometer DHR-2 (TA Instrument Inc., DE, USA), adopting a cone-plate configuration and setting a gap distance of 0.1 mm. The tests were performed under steady conditions at a constant temperature of 24 °C in a range of shear strain between 0.1 to 100 s^{-1}. Moreover, the evolution of the viscosity as a function of time was investigated at 24 °C and constant angular frequency of 100 rad/s. In both cases, data were taken after 30 s of soaking time.

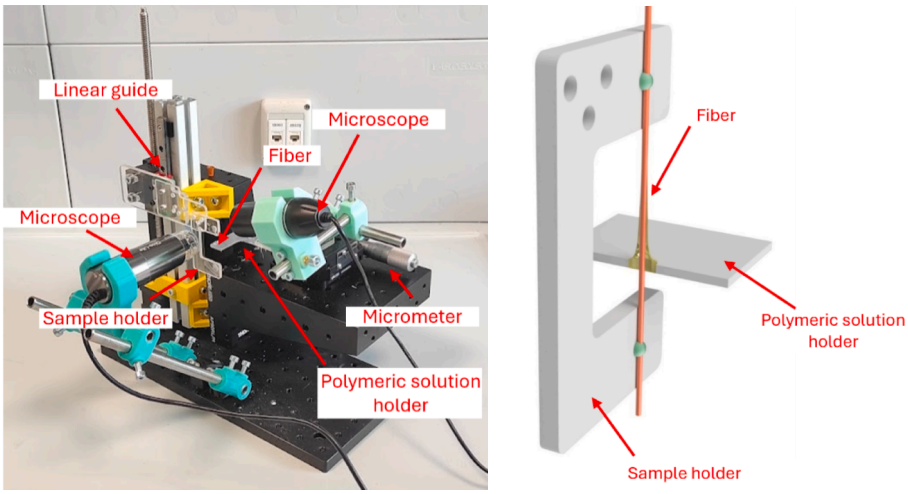

Fig. 1. (a) Custom-built apparatus for coating deposition on fiber and (b) graphical representation of the fiber on the sample holder during the process.

Table 1
Samples codes.

Samples codes	Type of coating	Speed (mm/s)
BF	–	–
BF_PCL_1.5	PCL	1.5
BF_PCL_3.5	PCL	3.5
BF_PCL_7	PCL	7
BF_PCL_14	PCL	14
BF_PCL_20	PCL	20
BF_PCL_30	PCL	30
BF_PCL_40	PCL	40
BF_PBAT_1.5	PBAT	1.5
BF_PBAT_3.5	PBAT	3.5
BF_PBAT_7	PBAT	7
BF_PBAT_14	PBAT	14
BF_PBAT_20	PBAT	20
BF_PBAT_30	PBAT	30
BF_PBAT_40	PBAT	40
BF_PBAT_50	PBAT	50
BF_PBAT_80	PBAT	80
BF_PBAT_90	PBAT	90
BF_PBAT_100	PBAT	100

2.3.2. Scanning electron microscopy

The morphological analysis of the as received and coated fibers was carried out using a Zeiss Supra 40 field-emission scanning electron microscope (FESEM) (Carl Zeiss AG, Oberkochen, Germany). Prior to the analysis, the samples were metallized with a platinum/palladium (Pt/Pd) alloy (80:20) layer of 5 nm thick. Coating thickness was measured from SEM pictures using ImageJ (version 1.53a), by comparing the coated fibers with the uncoated ones.

2.3.3. Contact angle measurements

The contact angle analysis was carried out by the dynamic contact angle technique in water by using a Thermo Cahn DCA 322 tensiometer (Bridge Tronic Global Inc, Irvine, USA) in an advancing and receding cycle. The water was contained in a small bath and the fiber attached vertically on a clamp. The tests were performed at an advancing/receding speed of 20 μm/s with a maximum immersion depth of 10 mm. The tensiometer measures the mass m during the test and the contact angle θ is derived from the Wilhelmy relationship (Equation (1), where F_c is the capillary force, g is the gravity acceleration, p is the wetted length, γ_L is the surface tension of water (72.60 mN/m, [47]). Results are presented with confidence level of 95 %.

$$F_c = m \bullet g = p\gamma_L cos\theta \quad (1)$$

In particular, two contact angles (CAs) were measured, an advancing contact angle (Θ_{ACA}) and a receding contact angle (Θ_{RCA}) that represent the highest and the lowest stable CAs values, respectively. The hysteresis angle (Θ_H) was calculated as reported in Equation (2).

$$\Theta_H = \Theta_{ACA} - \Theta_{RCA} \quad (2)$$

2.3.4. Microdebonding tests

The interfacial shear strength (IFSS) values were measured in microdebonding configuration by using an Instron 4502 tensile machine (Instron, USA) equipped with a 2.5 N load cell. PCL and PBAT droplets were deposited on basalt fibers at a coating speed higher than 20 mm/s for PCL and higher than 80 mm/s for PBAT. Therefore, PCL/BF and PBAT/BF microcomposites were prepared and tested to assess the PCL and PBAT adhesion level with BF. Droplet lengths between 60 to 250 μm were measured from collected SEM pictures using the software ImageJ (version 1.53a). On the other hand, epoxy droplets were manually applied and cured on individual as received and coated fibers to obtain EP/BF, EP/(PCL-coated BF) and EP/(PBAT-coated BF) microcomposites. In this case, the lengths of the epoxy droplets were between 50 and 130 μm. Force data were recorded during the microdebonding at a displacement rate of 0.75 mm/min. A comprehensive description of the device and methodology employed can be found in Simonini et al [28]. Approximately 3–5 droplets were debonded on each fiber, with a total of three fibers tested per sample, resulting in a cumulative dataset of approximately 9–15 debonded droplets per sample.

The IFSS is obtained as reported in Equation (3):

$$IFSS = \frac{F_{max}}{\pi d l} \quad (3)$$

F_{max} represents the maximum shear load registered during the microdebonding test, d is the diameter of the fiber, and l is the droplet's length. After being debonded, the epoxy droplets were healed by placing the microcomposites in an oven. Uncoated samples (i.e. EP/BF) were healed at 80 °C for 30 min and at 120 °C for 30 min and they were used as reference values for the coated ones. Samples coated with PCL were healed at 80 °C for 30 min whereas sample coated with PBAT were healed at 120 °C for 30 min. These healing temperatures were selected on the principles outlined by Karger-Kocsis et al. [48]. After cooling at room temperature, the healed microcomposites were re-tested as previously described. The healed samples were identified by adding the letter H after the codes listed in Table 1. The healing efficiency (HE) was calculated as the ratio between the interfacial shear strength after healing ($IFSS_H$) and its initial value (IFSS), as reported in Equation (4):

$$HE = \frac{IFSS_H}{IFSS} \bullet 100 \quad (4)$$

3. Results

3.1. Characterization of the polymer solutions

Fig. 2a shows the shear stress as a function of shear rate for the polymer solutions with PCL and PBAT, while Fig. 2b shows their viscosity values as a function of time.

Form Fig. 2a, PCL solution displays a linear increase in shear stress with shear rate, which is typical for a Newtonian fluid [49]. This means that the viscosity of PCL remains constant regardless of the shear rate. As the shear rate increases, as would occur during the coating process, the shear stress increases proportionally, but the viscosity remains unchanged. This consistent flow behaviour makes PCL a reliable material for coating processes, as it allows for a uniform application of the coating. At higher speeds, the material will behave predictably, leading to more consistent coating thicknesses. In contrast, PBAT has a shear-thinning behaviour whose shear stress decreases under shear rate allowing it to flow and spread more easily at higher speeds, which should result in coatings thinner than those with PCL at the same deposition rate. However, due to the reduced viscosity at higher shear rates, achieving uniform film thicknesses can be more challenging compared to PCL, as the material becomes more fluid and less stable under higher shear rate conditions [46].

From Fig. 2b, PCL exhibits a fairly steady increase in viscosity over time due to solvents evaporation, while PBAT exhibits a more stable viscosity that does not vary significantly throughout the experiment. The different behaviour of PBAT may be attributed to its copolyester structure that possibly results in weaker interaction with solvents [50]. However, since the deposition process takes approximately 5 min, it is reasonable to consider the viscosity as practically constant for both polymeric solutions.

3.2. Characterization of the uncoated and coated fiber surface

Fig. 3 reports the SEM pictures of as received and PCL/PBAT coated basalt fibers at various coating speeds between 1.5 and 14 mm/s. In Table 2, the mean and standard deviations of coating thickness measured from the SEM pictures are reported.

From Fig. 3, the surface of the as received basalt fiber (BF) appears relatively smooth, with some minor irregularities, typical of natural fibers. This serves as a baseline for comparing the effects of the coating process on the fiber's surface. As the coating is applied at faster speeds (from 1.5 to 14 mm/s), a gradual increase in thickness can be observed [44]. At the lowest speed (1.5 mm/s), the PCL coating is relatively thin (0.13 ± 0.02 μm) and appears somewhat discontinuous, with some areas showing minimal coverage. As the deposition speed increases (3.5 and 7 mm/s), the coating becomes more uniform and thicker (0.15 ± 0.01 μm and 0.36 ± 0.06 μm), as evidenced by a smooth and continuous coating layer. At the highest speed (14 mm/s), the PCL coating is significantly thicker (0.66 ± 0.04 μm) and more homogeneous, with a well-defined and smooth surface. This is consistent with the previously discussed trend of increased coating thickness with higher deposition speeds, likely due to the Newtonian nature of PCL. Also for PBAT coatings, a trend of increasing coating thickness with higher deposition speeds is observed. However, as expected from the different rheological behaviour, the PBAT coating appears to be thinner and less uniform compared to PCL at the same deposition speeds [46]. At the lowest speed (1.5 mm/s), the coating is very thin (0.08 ± 0.02 μm) and uneven, with some visible gaps or discontinuities. As the speed increases (3.5, 7, 14 mm/s), the PBAT coating becomes more continuous, but it still remains thinner compared to the PCL coatings (0.16 ± 0.05 μm, 0.17 ± 0.02 μm ad 0.27 ± 0.01 μm, respectively). This behaviour is likely due to the shear thinning nature of PBAT, which allows the fluid to spread more easily at higher speeds, but results in a thinner layer due to the rapid flow and reduced spreading resistance. Therefore, according to the fluid coating theory, the differences in fluid behaviour of PCL and PBAT result in distinct coating profiles for the two materials. This highlights the importance of considering fluid rheology in the design of a coating processes.

Fig. 4(a-c) shows an example of a complete cycle (advancing, static and receding) for a contact angle test in water on a BF, BF_PCL_14 and BF_PBAT_14 samples. The testing setup is shown in Fig. 4d. The values of contact angle are reported in Table 3.

The Θ_{ACA} values shows little variation among samples with values of 70.3° ± 0.8 for BF, 69.5° ± 0.9 for BF_PCL_14 and 72.4° ± 0.1 for BF_PBAT_14. These similarities indicate that the application of PCL and PBAT coatings has no substantial effect on the slight hydrophilic nature of as received basalt fibers. In contrast, the Θ_{RCA} varies significantly, highlighting differences in surface properties such as roughness, coating uniformity, and liquid pinning behaviour [51]. BF exhibits a low Θ_{RCA} of 38.2° ± 0.1, indicating pinning of the water droplet due to a quite heterogeneous surface morphology. For BF_PCL_14, the Θ_{RCA} increases to 52.5° ± 0.9, suggesting that the PCL coating reduces surface heterogeneity. BF_PBAT_14 shows the highest Θ_{RCA} at 70.6° ± 0.8, nearly matching its Θ_{ACA} value, indicating minimal pinning due to the highly uniform and smooth PBAT coating [51]. About Θ_H, BF exhibit a high hysteresis of 32.1°, consistent with surface heterogeneity. For BF_PCL_14, the hysteresis decreases to 17.0°, reflecting the smoother surface created by the PCL coating. BF_PBAT_14 has an extremely low hysteresis of 1.8°, resulting in a highly uniform surface.

The morphological aspect of PCL and PBAT droplets obtained at coating speeds above 20 mm/s for PCL and 80 mm/s for PBAT is reported in Figs. 5 and 6(a,b). The measured droplet lengths are reported

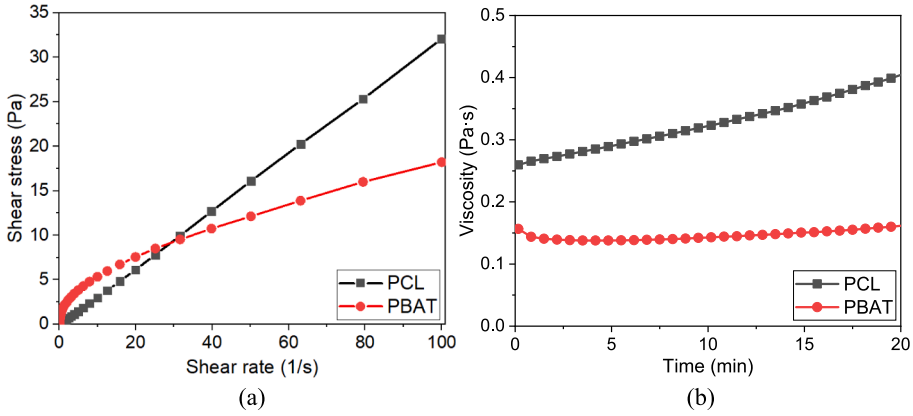

Fig. 2. Rheological curves of PCL and PBAT solutions: (a) shear stress as a function of shear rate, and (b) viscosity as a function of time.

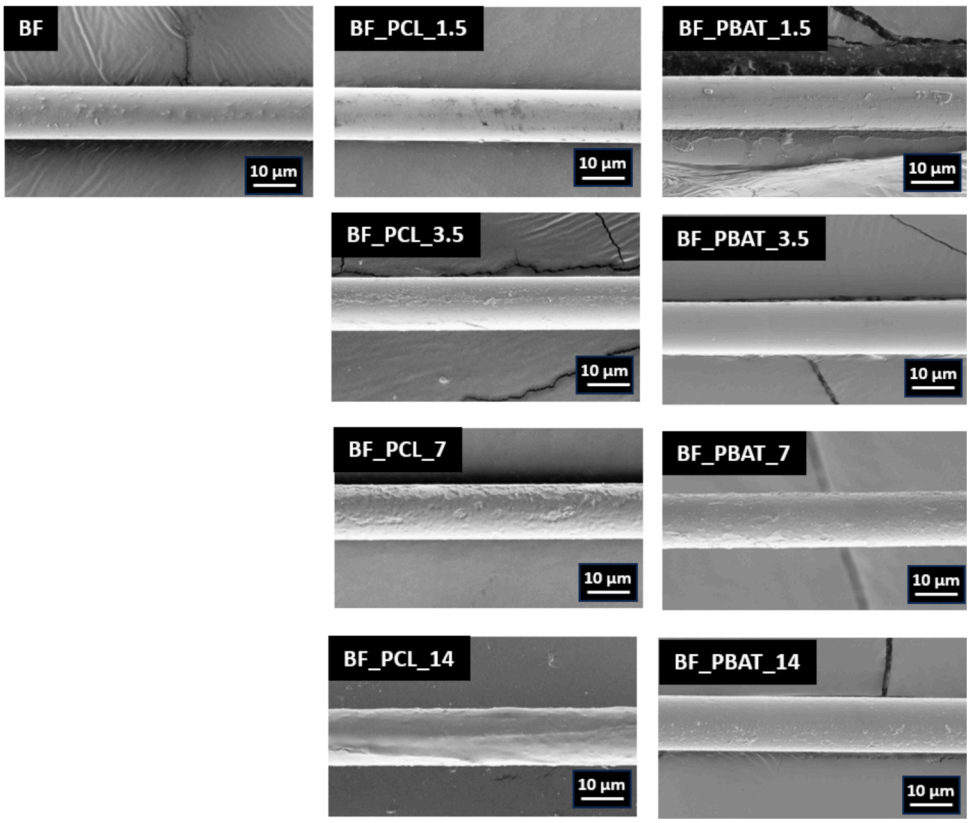

Fig. 3. SEM pictures of the morphology of as received and (PCL/PBAT)-coated basalt fibers as a function of the coating speed.

Table 2
Value of coating thickness of (PCL/PBAT)-coated basalt fibers.

Samples	Thickness (µm)
BF	–
BF_PCL_1.5	0.13 ± 0.02
BF_PCL_3.5	0.15 ± 0.01
BF_PCL_7	0.36 ± 0.06
BF_PCL_14	0.66 ± 0.04
BF_PBAT_1.5	0.08 ± 0.02
BF_PBAT_3.5	0.16 ± 0.05
BF_PBAT_7	0.17 ± 0.02
BF_PBAT_14	0.27 ± 0.01

in Table 4.

According to Fig. 5, the PCL droplets obtained at 20 mm/s are relatively small (134 ± 9 µm), uniformly spaced, and have a uniform morphology and size. The transition from continuous coatings (Fig. 3) to droplets (Fig. 5) represents the onset of capillary instability, where inertial effects begin to influence fluid deposition due to increasing coating speed. The periodic rupture of the liquid film into droplets follows the behaviour described by the Rayleigh instability theory, in which the coating fluid rearranges itself into droplets to minimise surface energy [44]. At 30 mm/s, this droplet effect is largely evident and the droplets begin to enlarge and slightly elongate (146 ± 8 µm). As the coating velocity continues to increase up to 40 mm/s, inertial forces play a greater role, causing a larger volume of liquid film to break into distinct droplets (215 ± 24 µm). The observed morphology is consistent with Newtonian fluid coating theory, where higher velocities lead to less liquid diffusion and more pronounced Rayleigh instability, pushing the liquid toward droplet formation rather than uniform coating. In contrast, PBAT droplets exhibit a different behaviour. The droplet size remains relatively consistent regardless the coating speeds, which is directly correlated with the shear-thinning nature of PBAT. As a result, PBAT forms droplets of rather similar size (from 84 ± 11 µm to 120 ± 10 µm) even as the coating speed increases (80, 90, 100 mm/s). Additionally, at lower speeds (20, 30, 40 and 50 mm/s) (Fig. S1 in supplementary materials), PBAT does not form distinct droplets but instead creates a continuous coating along the basalt fibers. This behaviour can be attributed to the reduced viscosity at higher shear rates, which allows the fluid to flow more easily along the fiber surface, preventing the capillary-driven breakup observed in PCL coatings. The shear-thinning nature of PBAT thus suppresses droplet formation at lower speeds and promotes a more uniform and continuous coating, while at higher speeds, the reduced viscosity limits significant variation in droplet size. Additionally, Fig. 6(a,b) reveals morphological differences between the PCL and PBAT droplets. In the BF_PCL_20 sample (Fig. 6a), the PCL droplet appears relatively rough and irregular. This morphology suggests the presence of porosity, most likely caused by a slight solvent evaporation during the coating or drying process. The slight solvent loss detected in rheological tests (Fig. 2b) supports this observation, as evaporation can lead to localized shrinkage and pore formation. These irregularities not only affect the visual appearance but possibly could also influence the interfacial adhesion properties by creating microdefects at the fiber-coating interface. In contrast, the BF_PBAT_100 sample (Fig. 6b) shows a pore-free droplet's morphology. This difference can be attributed to the absence of significant solvent evaporation in PBAT, as indicated by rheological data (Fig. 2b).

Fig. 7(a, b) shows the load–displacement curves obtained from microdebonding tests on PCL and PBAT droplets. In Table 5, the mean and standard deviation values of IFSS are summarized.

The load–displacement curves for PCL and PBAT droplets highlight differences in the interfacial behaviour and debonding mechanisms. For PCL-droplets, the curves exhibit progressive loading up to a maximum load, followed by a sharp drop in force, indicating an abrupt interfacial failure. The curves for BF_PCL_20, BF_PCL_30, and BF_PCL_40 display

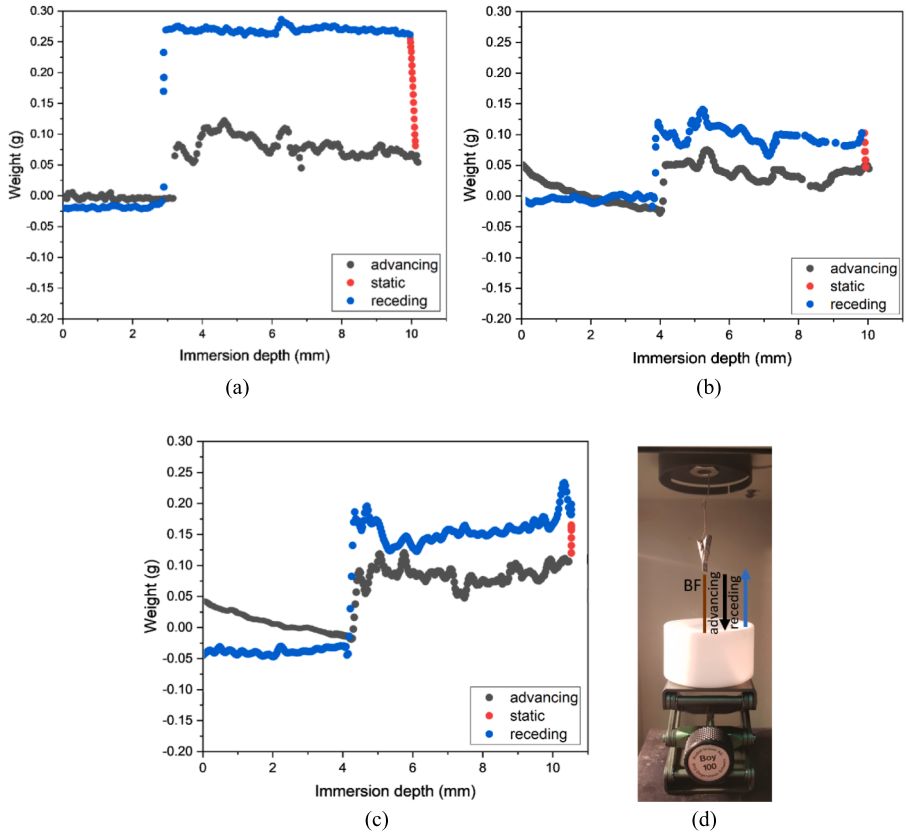

Fig. 4. Example of a complete cycle (advancing, static and receding) for a contact angle test in water on (a) BF, (b) BF_PCL_14 and (c) BF_PBAT_14 samples, while (d) is the testing setup used.

Table 3
Values of contact angle.

Samples	Θ_{ACA} (°)	Θ_{RCA} (°)	Θ_{H} (°)
BF	70.3 ± 0.8	38.2 ± 0.1	32.1
BF_PCL_14	69.5 ± 0.9	52.5 ± 0.9	17.0
BF_PBAT_14	72.4 ± 0.1	70.6 ± 0.8	1.8

similar trends with slight differences in peak loads and displacements. This suggests a relatively uniform interfacial strength across the different coating speeds. The calculated IFSS values further corroborate this observation, with values of 10.70 ± 1.54 MPa, 10.05 ± 3.54 MPa, and 10.31 ± 0.38 MPa, respectively. The similarity in IFSS values, despite differences in droplet size, reflects consistent wetting and adhesion behaviour for PCL. In contrast, for PBAT-droplets, the load–displacement curves exhibit distinct characteristics. The force increases to a peak, but decreases more gradually than in PCL, suggesting a more progressive debonding process and thus a more ductile failure mode or greater energy dissipation during debonding. The IFSS values for BF_PBAT_80, BF_PBAT_90, and BF_PBAT_100 are notably lower than those for PCL-coated fibers, with values of 6.45 ± 0.81 MPa, 6.13 ± 0.54 MPa, and 6.81 ± 0.86 MPa, respectively. Additionally, the frictional plateau, which is the region of the curve after the initial increase in load where the force becomes constant, appears to be the same across

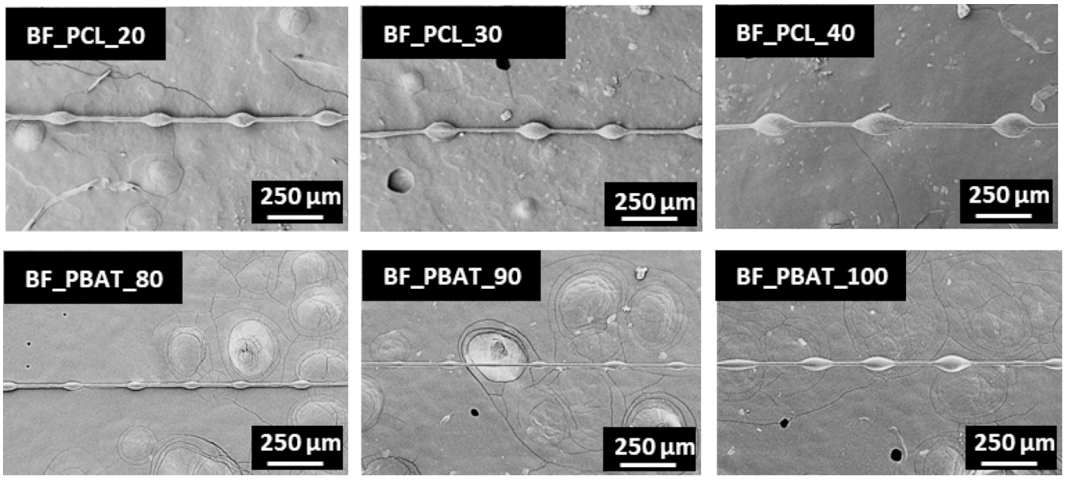

Fig. 5. Morphological aspect of PCL and PBAT droplets as a function of coating speed.

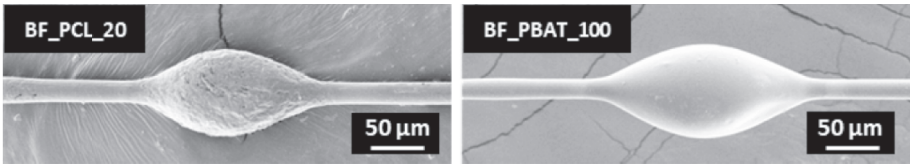

Fig. 6. Detailed morphology of single droplet of (a) PCL and (b) PBAT.

Table 4
Lengths of PCL and PBAT droplets.

Samples	Size (µm)
BF_PCL_20	134 ± 9
BF_PCL_30	146 ± 8
BF_PCL_40	215 ± 24
BF_PBAT_80	84 ± 11
BF_PBAT_90	88 ± 18
BF_PBAT_100	120 ± 10

all the samples. This indicates that the frictional resistance encountered by the droplets along the BF surface after the debonding is consistent for all the tested conditions.

3.3. Evaluation of the epoxy/fiber interfacial adhesion and healing efficiency

Fig. 8(a-c) shows the load–displacement curves as measured from microdebonding tests on EP/BF, EP/(PCL-coated BF) and EP/(PBAT-coated BF) microcomposites, before and after healing. In Table 6, the mean and standard deviation values of IFSS and HE are summarized.

From Fig. 8a, the uncoated basalt fiber microcomposite (EP/BF) displays an IFSS of 45.8 ± 3.1 MPa and a load–displacement curve characterized by a steady increase in load until a sharp peak at approximately 0.30 N, followed by a sudden drop indicating interfacial failure. Upon healing (EP/BF_H), the maximum load capacity is significantly reduced, with a broad peak load around 0.05 N and a negligible healing efficiency (HE) of 5.3 ± 2.6 % at 80 °C and 7.6 ± 2.9 % at 120 °C (due to some residual curing of EP at higher temperature) confirming that the EP/BF system lacks self-healing properties. For PCL coated fibers (EP/BF_PCL_7 and EP/BF_PCL_14) in Fig. 8b, the load–displacement curves show an initial load increase similar to that of the uncoated fibers, with comparable IFSS values (40.2 ± 5.8 MPa and 42.1 ± 1.1 MPa, respectively), indicating that the presence of the coating maintains the interfacial adhesion properties without negatively altering them. After healing, both samples (EP/BF_PCL_7_H and EP/BF_PCL_14_H) retain a substantial portion of their original load-bearing capacity, with EP/BF_PCL_14_H nearly matching its initial performance. The healing efficiencies are notably high, at 83.9 ± 6.6 % for EP/BF_PCL_7 and 100.8 ± 2.7 % for EP/BF_PCL_14, suggesting that the thicker PCL coating provides a more effective polymer reservoir for healing through thermal activation. In contrast, PBAT-coated fibers (EP/BF_PBAT_7 and EP/BF_PBAT_14) exhibit moderate behavior. The load–displacement curves in Fig. 8c show that EP/BF_PBAT_7 achieves a higher peak load compared to EP/BF_PBAT_14, likely due to differences in coating morphology or thickness. The IFSS values for these samples are 49.7 ± 8.8 MPa for EP/BF_PBAT_7 and 36.1 ± 3.3 MPa for EP/BF_PBAT_14. This suggests that the thinner PBAT coating may leave parts of the fiber's rough surface exposed, enhancing mechanical interlocking, whereas a thicker coating smoothens the surface and reduces adhesion. After healing (EP/BF_PBAT_7_H and EP/BF_PBAT_14_H), both samples demonstrate a significant recovery in load-bearing capacity. The healing efficiencies are 69.9 ± 8.8 % for EP/BF_PBAT_7 and 89.5 ± 6.4 % for EP/BF_PBAT_14. Although these values are slightly lower than those observed in PCL-coated samples, they still reflect impressive healing capabilities. Finally, the friction plateau of the microdebonding curves is slightly lower after healing for all sample types. This may be due to a smoothening of the coating roughness after thermal healing, as observed in previous works by our group on PCL coatings [28,38].

4. Conclusions

In this study, the interfacial properties and healing capabilities of basalt fiber-reinforced composites were enhanced through the application of thermoplastic polymer coatings on basalt fibers using a fluid

Table 5
Values of IFSS of PCL/BF and PBAT/BF microcomposites.

Samples	IFSS (MPa)
BF_PCL_20	10.7 ± 1.5
BF_PCL_30	10.1 ± 3.5
BF_PCL_40	10.3 ± 0.4
BF_PBAT_80	6.5 ± 0.8
BF_PBAT_90	6.1 ± 0.5
BF_PBAT_100	6.8 ± 0.8

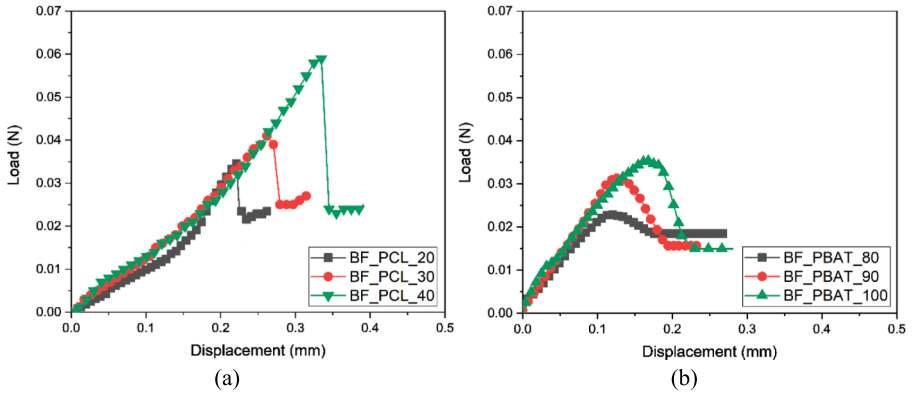

Fig. 7. Load-displacement curves form microdebonding tests on (a) PCL/BF and (b) PBAT/BF microcomposites.

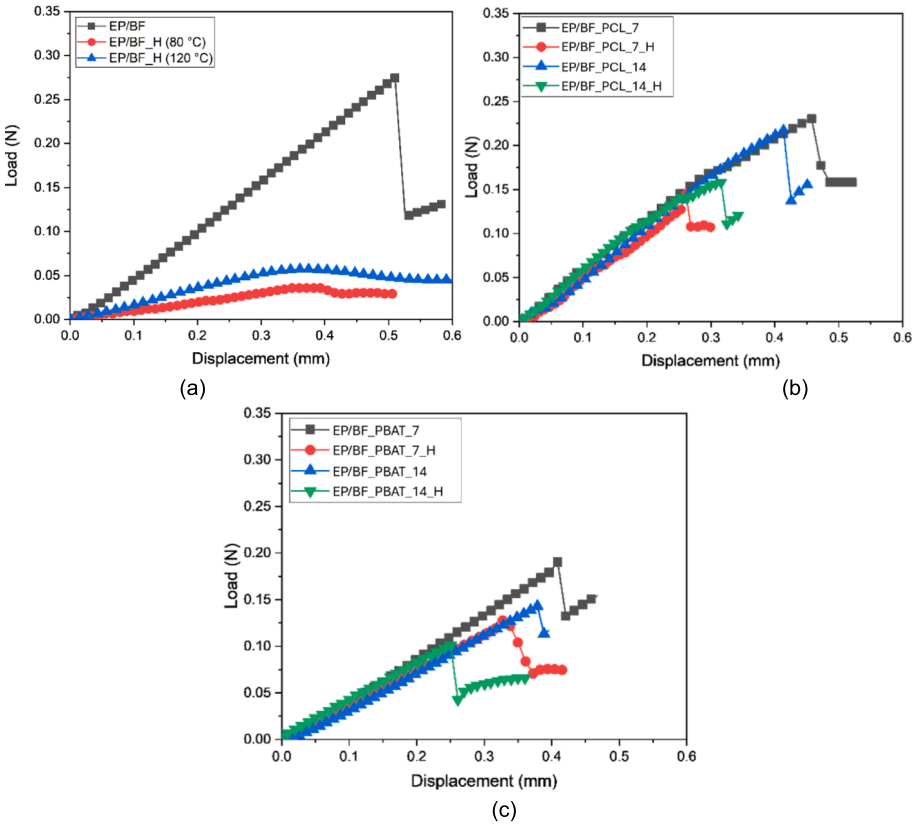

Fig. 8. Load-displacement curves form microdebonding tests on (a) EP/BF, (b) EP/(PCL-coated BF) and (c) EP/(PBAT-coated BF) microcomposites.

Table 6
Values of IFSS and HE of EP/BF, EP/PCL-coated BF and EP/PBAT-coated BF microcomposites.

Samples	IFSS (MPa)	HE (%) at 80 °C	HE (%) at 120 °C
EP/BF	45.8 ± 3.1	5.3 ± 2.6	7.6 ± 2.9
EP/BF_PCL_7	40.2 ± 5.8	83.9 ± 6.6	–
EP/BF_PCL_14	42.1 ± 1.1	93.8 ± 2.7	–
EP/BF_PBAT_7	49.7 ± 8.8	–	69.9 ± 8.8
EP/BF_PBAT_14	36.1 ± 3.3	–	89.5 ± 6.4

coating approach. In particular, poly(butylene adipate-co-terephthalate) (PBAT) was investigated as a possible alternative to the widely investigated polycaprolactone (PCL). The two polymers displayed distinct rheological behaviours, i.e. Newtonian for PCL and shear-thinning for PBAT. The two polymers were successfully deposited on the fibers and their morphologies were analyzed through SEM analysis, revealing rather smooth and uniform layers at lower coating speeds, with droplet formation observed at higher speeds. Contact angle measurements provided additional insights into the surface properties of the coated fibers. The advancing contact angle (Θ_{ACA}) remained relatively consistent across all samples, indicating similar surface characteristics. However, the receding contact angle (Θ_{RCA}) varied significantly, especially for PBAT-coated fibers, which exhibited higher Θ_{RCA} values. The hysteresis (Θ_H) between advancing and receding angles was lowest in PBAT-coated samples, reflecting their more uniform surface characteristics compared to PCL-coated and uncoated fibers. The interfacial shear strength (IFSS) measurements on EP/(coated BF) indicated that while the polymer coatings slightly influenced adhesion, they did not drastically alter the IFSS compared to uncoated fibers. Load-displacement curves confirmed the self-healing behaviour for coated BF, with PBAT-coated composites displaying a recovery comparable to that of PCL-coated fibers. Despite PBAT's slightly lower healing efficiency, it still provided notable repair capabilities, highlighting the potential of both thermoplastic coatings in extending the durability of fiber-reinforced composites. Overall, this work demonstrated that thermoplastic polymer coatings significantly improved the healing capability of basalt fiber-reinforced composites without compromising interfacial strength. The application of fluid coating theory to deposit these polymers provided a scalable and effective strategy for developing advanced, healable composite materials suitable for demanding structural applications.

CRediT authorship contribution statement

Laura Simonini: Writing – review & editing, Writing – original draft, Visualization, Validation, Methodology, Investigation, Formal analysis, Data curation, Conceptualization. **Daniele Rigotti:** Writing – review & editing, Visualization, Software, Methodology, Investigation. **Jeevan Kishore Reddy Pidapa:** Visualization, Investigation, Formal analysis, Data curation. **Alessandro Pegoretti:** Writing – review & editing, Visualization, Validation, Supervision, Resources, Conceptualization.

Declaration of competing interest

The authors declare that they have no known competing financial interests or personal relationships that could have appeared to influence the work reported in this paper.

Appendix A. Supplementary data

Supplementary data to this article can be found online at https://doi.org/10.1016/j.compositesa.2025.109010.

Data availability

Data will be made available on request.

References

[1] Ozturk F, Cobanoglu M, Ece RE. Recent advancements in thermoplastic composite materials in aerospace industry. *J Thermoplast Compos Mater* 2024;37:3084–116.
[2] Koniuszewska AG, Kaczmar JW. Application of polymer based composite materials in transportation. *Prog Rubber Plast Recycl Technol* 2016;32:1–24.
[3] Zaman A, Gutub SA, Wafa MA. A review on FRP composites applications and durability concerns in the construction sector. *J Reinf Plast Compos* 2013;32:1966–88.
[4] Mohanty AK, Vivekanandhan S, Pin JM, Misra M. Composites from renewable and sustainable resources: Challenges and innovations. *Sci Sinter* 2018;326:536–42.
[5] Abouelleil H, Pradelle N, Villat C, Attik N, Colon P, Grosgogeat B. Comparison of mechanical properties of a new fiber reinforced composite and bulk filling composites. *Restorative Dentistry Endodontics* 2015;40:262–70.
[6] Silu, H.; Bo, W.; Libo, Y. Interphase and interfacial properties of composite materials. In *Composite Materials: Manufacturing, Properties and Applications*; Elsevier, Ed., **2021**; pp. 151-177.
[7] Dharmavarapu P, MBS SR. Aramid fibre as potential reinforcement for polymer matrix composites: a review. *Emergent Materials* 2022;5:1561–78.
[8] Da Silva, L.; Ochsner, A.; Adams, R. *Handbook of Adhesion Technology*. vol. *1*, **2011**.
[9] Ahmad H, Markina AA, Porotnikov MV, Ahmad F. A review of carbon fiber materials in automotive industry. *Mater Sci Eng* 2020;971:1–11.
[10] Ash JT, Cross WM, Svalstad D, Kellar JJ, Kjerengtroen L. Finite element evaluation of the microbond test: meniscus effect, interphase region, and vise angle. *Compos Sci Technol* 2003;63:641–51.
[11] Chen J, Zhu Y, Ni Q, Fu Y, Fu X. Surface modification and characterization of aramid fibers with hybrid coating. *Appl Surf Sci* 2014;321:103–8.
[12] Xu L, Drzal LT. Improvement of adhesion between vinyl ester resin and carbon fibers. In: In *Proceedings of the 13th International Conference on Composite Materials*; 2013. p. 1–10.
[13] Cai G, Wada M, Ohsawa I, Kitaoka S, Takahashi J. Influence of treatment with superheated steam on tensile properties of carbon fiber. *Compos A Appl Sci Manuf* 2018;107:555–60.
[14] Khandelwal S, Rhee K. Recent advances in basalt-fiber-reinforced composites: Tailoring the fiber-matrix interface. *Compos B Eng* 2020;192:108011–24.
[15] Raphael N, Namratha K, Chandrashekar BN, Sadasivuni KK, Ponnamma D, Smitha AS, et al. Surface modification and grafting of carbon fibers: A route to better interface. *Prog Cryst Growth Charact Mater* 2018;64:75–101.
[16] Mahmood H, Simonini L, Dorigato A, Pegoretti A. Graphene deposition on glass fibers by triboelectrification. *Appl Sci* 2021;11:3123–34.
[17] Pozueco S, Simonini L, Mahmood H, Rigotti D, Kakkonen M, Riveiro A, et al. Influence of CO_2 laser surface treatment of basalt fibres on the mechanical properties of epoxy/basalt composites. *Polym Compos* 2024. In press.
[18] Simonini L, Mahmood H, Dorigato A, Pegoretti A. Tailoring the physical properties of poly (lactic acid) through the addition of thermoplastic polyurethane and functionalized short carbon fibers. *Polym Compos* 2023;44:4719–33.
[19] Sharma, M.; Gao, S.; Mader, E.; H., S.; Wei, L.Y.; Bijwe, J. Carbon fiber surfaces and composite interphases. *Carbon fiber surfaces and composite interphases* **2014**, *102*, 35-50.
[20] Jones AR, Blaiszik BJ, White SR, Sottos NR. Full recovery of fiber/matrix interfacial bond strength using a microencapsulated solvent-based healing system. *Compos Sci Technol* 2013;79:1–7.
[21] Simonini L, Kakkonen M, Dsouza R, Kanerva M, Mahmood H, Dorigato A, et al. Tailoring the interfacial properties of glass fiber-epoxy microcomposites through the development of a self-healing poly (ε-caprolactone) coating. *Compos Sci Technol* 2024;261:110991–1007.
[22] Cohades A, Branfoot C, Rae S, Bond I, Michaud V. Progress in Self-Healing Fiber-Reinforced Polymer Composites. *Adv Mater Interfaces* 2018;5.
[23] Blaiszik BJ, Kramer SL, Olugebefola SC, Moore JS, Sottos NR, White SR. Self-healing polymers and composites. *Annu Rev Mat Res* 2010;40:179–211.
[24] Patrick J, Robb M, Sottos N, Moore J, White S. Polymers with autonomous life-cycle control. *Nature* 2016;540:363–70.
[25] Dhand V, Mittal G, Rhee K, Park S, Hui D. A short review on basalt fiber reinforced polymer composites. *Compos B Eng* 2015;73:166–80.
[26] Jamshai H, Mishra R. A green material from rock: basalt fiber–a review. *J Textile Institute* 2016;107:923–37.
[27] Greco A, Maffezzoli A, Casciaro G, Caretto F. Mechanical properties of basalt fibers and their adhesion to polypropylene matrices. *Compos B Eng: Eng* 2014;67:233–8.
[28] Simonini L, Mahmood H, Dorigato A, Pegoretti A. Evaluation of self-healing capability of a polycaprolactone interphase in epoxy/glass composites. *Compos A Appl Sci Manuf* 2023;169:107539–48.
[29] Kosarli M, Bekas DG, Tsirka K, Baltzis D, Vaimakis-Tsogkas DT, Orfanidis S, et al. Microcapsule-based self-healing materials: Healing efficiency and toughness reduction vs. capsule size. *Compos B Eng* 2019;171:78–86.
[30] Mahmood H, Dorigato A, Pegoretti A. Healable carbon fiber-reinforced epoxy/cyclic olefin copolymer composites. *Materials* 2020;13:2165–80.
[31] Norris CJ, Meadway GJ, O'Sullivan MJ, Bond IP, Trask RS. Self-healing fibre reinforced composites via a bioinspired vasculature. *Adv Funct Mater* 2011;21:3624–33.
[32] Pearson A, Liao W, Kazemi Y, Duncan M, Slingerland E, Kakroodi A, et al. Fiber-matrix adhesion between high-density polyethylene and carbon fiber. *Polym Test* 2022;105.
[33] Zhang W, Duchet J, Gerard JF. Self-healable interfaces based on thermo-reversible Diels–Alder reactions in carbon fiber reinforced composites. *J Colloid Interface Sci* 2014;430:61–8.
[34] Zheng S, Lü H, Chen C, Nie K, Guo Q. Epoxy resin/poly (ethylene oxide)(PEO) and poly (ε-caprolactone)(PCL) blends cured with 1, 3, 5-trihydroxybenzene: miscibility and intermolecular interactions. *Colloid Polym Sci* 2003;281:1015–24.
[35] Cohades A, Manfredi E, Plummer CJG, Michaud V. Thermal mending in immiscible poly(ε-caprolactone)/epoxy blends. *Eur Polym J* 2016;81:114–28.
[36] Cohades A, Michaud V. Thermal mending in E-glass reinforced poly (ε-caprolactone)/epoxy blends. *Compos A Appl Sci Manuf* 2017;99:129–38.
[37] Karger-Kocsis J. Self-healing properties of epoxy resins with poly(ε-caprolactone) healing agent. *Polym Bull* 2016;73:3081–93.
[38] Simonini L, Canale R, Mahmood H, Dorigato A, Pegoretti A. Multifunctional epoxy/carbon composites with a fully reparable interface. *Polym Compos* 2024;45:2558.
[39] Malikmammadov E, Tanir TE, Kiziltay A, Hasirci V, Hasirci N. PCL and PCL-based materials in biomedical applications. *J Biomater Sci Polym Ed* 2018;29:863–93.
[40] Mohamed RM, Yusoh K. A review on the recent research of polycaprolactone (PCL). In: In *Proceedings of the Advanced Materials Research*; 2016. p. 249–55.
[41] Burford T, Rieg W, Madbouly S. Biodegradable poly (butylene adipate-co-terephthalate)(PBAT). *Phys Sci Rev* 2023;8:1127–56.
[42] Roy S, Ghosh T, Zhang W, Rhim J. Recent progress in PBAT-based films and food packaging applications: A mini-review. *Food Chem* 2024;437:137822–39.
[43] Lyu J, Lee J, Han J. Development of a biodegradable polycaprolactone film incorporated with an antimicrobial agent via an extrusion process. *Sci Rep* 2019;9:20236–47.
[44] Quere D. Fluid coating on a fiber. *Annu Rev Fluid Mech* 1999;31:347–84.
[45] De Ryck A, Quéré D. Inertial coating of a fibre. *J Fluid Mech* 1996;311:219–37.
[46] Javidi M, Pope M, Hrymak A. Investigation on dip coating process by mathematical modeling of non-Newtonian fluid coating on cylindrical substrate. *Phys Fluids* 2016;28:1–12.
[47] Chen LY, Liu XL, Wang HB, Lian ZT, Dai XC, Ma T. The biochemical characteristics and fluid property change of the produced fluid after microbial enhanced oil recovery of district q in xinjiang oilfield. *Int Field Explorat Devel Conf* 2021;1:4890–900.
[48] Karger-Kocsis J. Self-healing properties of epoxy resins with poly (ε-caprolactone) healing agent. *Polym Bull* 2016;73:3081–93.
[49] Van Waeleghem T, Marchesini FH, Cardon L, D'hooge DR. Melt exit flow modelling and experimental validation for fused filament fabrication: From Newtonian to non-Newtonian effects. *J Manuf Process* 2022;77:138–50.
[50] Khatsee S, Daranarong D, Punyodom W, Worajittiphon P. Electrospinning polymer blend of PLA and PBAT: Electrospinnability–solubility map and effect of polymer solution parameters toward application as antibiotic-carrier mats. *J Appl Polym Sci* 2018;135:46486–95.
[51] Lin HP, Chen LJ. Direct observation of wetting behavior of water drops on single micro-scale roughness surfaces of rose petal effect. *J Colloid Interface Sci* 2021;603:539–49.